Future XL monopile foundation design for a 10 MW wind turbine in deep water

K.W. Hermans
J.M. Peeringa

December 2016
ECN-E--16-069

Acknowledgement

The author is grateful for the budget that was made available to carry out this study as part of the knowledge finance of ECN.

Contents

Summary

The monopile foundation is the dominating support structure type for offshore wind farms in construction today. It is anticipated that also in future wind farms the monopile will remain a preferred choice due to the manufacturing speed and installation experience. However, larger, heavier turbines are being developed and wind farms are being installed in deeper waters, testing the technical and economic limits of monopile foundations against other foundation types.

This report contains the results of an ECN internal knowledge project on future large monopile foundations. One of the main objectives was to create a preliminary design for a 10 MW support structure in 50 m water depth. This is a degree larger than the current designs in the industry and is aimed to put our current models to the test. The basic design features a foundation pile diameter of 9.3 m and a total steel mass above mudline of 1850 tons. The design has not been optimized but was subjected to an ultimate load, buckling and fatigue check. A global buckling check for a buckling failure mode twice the length of the support structure was not passed and the applicability and implications of this failure mode must be further investigated. The basic design passed all other ultimate load checks and fatigue check at the mudline. Largest diameter in the support structure is 9.3 m which is within manufacturing capabilities.

The second objective was to identify the limitations of current design methods and simulation tools. The soil-structure interaction can be modelled by lateral springs (PY curves) with the current tools available to ECN. However, for large diameter foundations other physical load bearing mechanisms are at play and the PY curves do not suffice for accurate soil-structure modelling. For a 9.3 m monopile, modelling the hydrodynamic loading by diffraction does not have a very large influence on the magnitude of the loads, hence Morison's equation may still be used without being too conservative. Finally, there are assumptions made in evaluating the fatigue damage by using an SN curve and Miner's rule.

1

Introduction

Ever since the first offshore wind farms were built, the monopile support structure has been a solid foundation choice. From a manufacturing standpoint the monopile is the easiest to fabricate and in optimizing for example welding processes tighter tolerances could be achieved and production volume could be increased. As the turbine size is ever increasing and offshore wind farms are placed in deeper waters, monopile diameters have been growing to accomplish the right stiffness. The limits of applicability of monopile support structures have been shifting. Not long ago, water depth more than 25 meters or 5+ MW class turbines were considered the tipping point towards jackets or other alternative support structures. Nowadays, 'XL monopiles' of over 1000 tons are produced with diameters up to 8 meters for water depths up to 30-35 meters (**Figure 1**). This leads to the questions: 'What are really the limits of monopile support structures'? And can we design a monopile for a future scenario of a 10 MW turbine at a site of 50m water depth?

In this report a simplified design methodology is set up and applied for a basic design for a 10 MW turbine at 50 m water depth. Ultimate loads, buckling and fatigue checks are performed, but no optimization or detailed design is carried out. Finally, an evaluation is made of the current simulation tools at use in ECN. Are they still valid for large diameter monopiles?

Figure 1: The world's heaviest monopile for Veja Mate offshore wind farm [1]

2

Preliminary design

2.1 Proposal design

The proposed preliminary design is drafted by taking inspiration of current designs in the waters. A conical section is incorporated in the monopile to reduce wave loads in the splash zone and account for the increase in bending moment towards the mudline. The taper angle, height at which the conical section should start and diameter at mudline are taken as design inputs. In **Table 1** and **Table 2** the geometric design parameters are given and the resulting preliminary design is sketched in **Figure 3**. The overall design methodology is presented in the scheme of **Figure 2**.

Figure 2: Design methodology

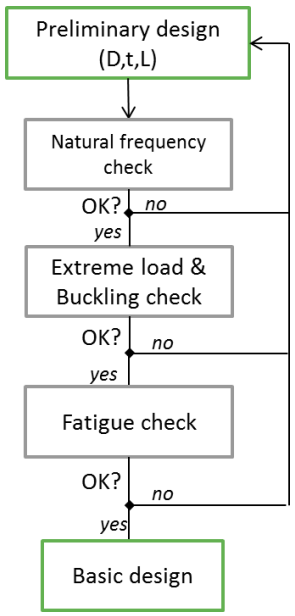

Table 1: Geometry variables used for 10 MW design rev 00

Description	value
Outer diameter at mudline	9.6 m
Height start taper MP above mudline	10 m
Length taper MP / taper angle MP	23.56 m / 2.5°
Top MP above mudline (bottom TP)	53.22 m
Platform height (top TP)	76.16 m
Height start taper tower above platform	10 m
Length taper tower / taper angle tower	47.96 m / 1.98°

Table 2: Diameter over thickness ratios used for 10 MW design rev 00

Description	value
D/t Monopile	100
D/t Transition Piece	80
D/t tower	140

Table 3: Mass for preliminary 10 MW design rev 00

Description	value
Mass of support structure steel (monopile above mudline, tower, transition piece)	1849 tons
Mass of internal water	2774 tons

Figure 3: Preliminary design rev 00

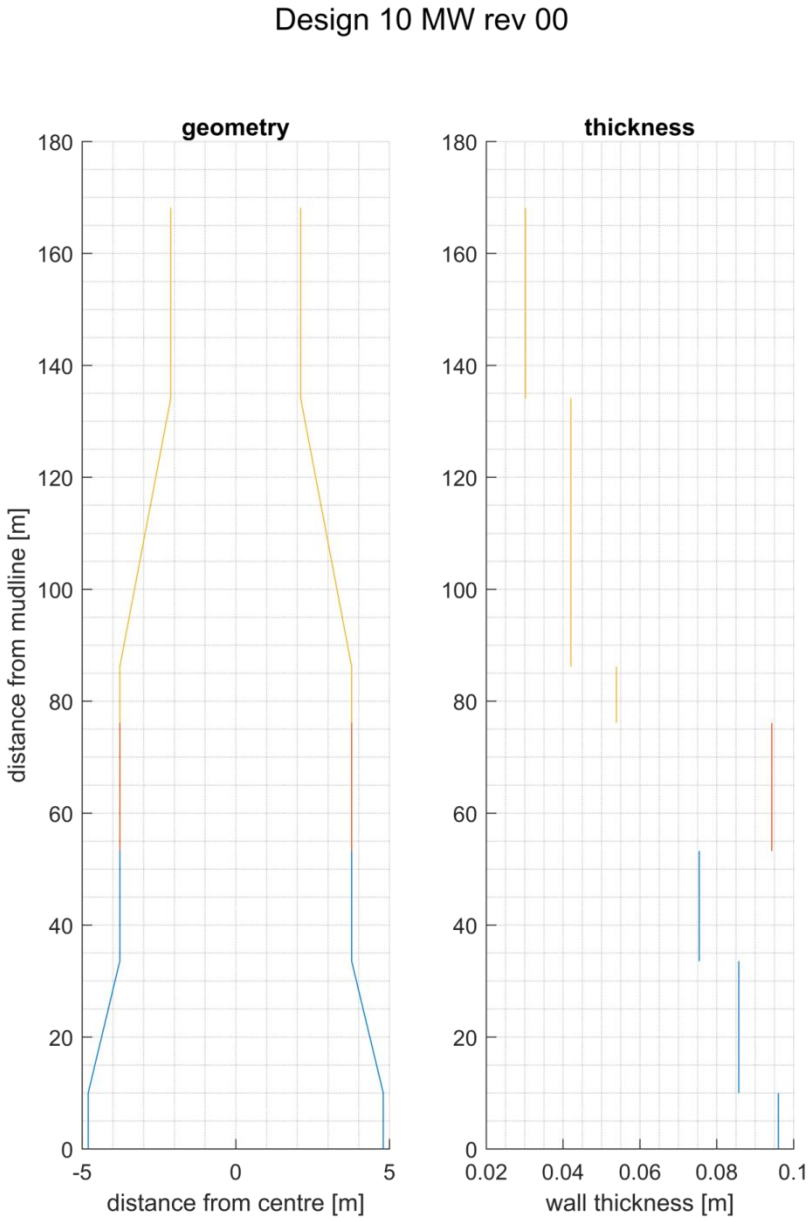

2.2 Foundation stiffness

In this first design iteration we limit ourselves to the design of the pile above the mudline. However in order to model the structural dynamics right, the foundation stiffness (and ideally also damping) must be taken into account. The soil layer properties of OC3 have been used, as reported by Passon [2]. The foundation model in Phatas includes a coupled lateral and rotation spring matrix. Recently, the Phatas soil-structure interaction model has been improved by adding a PY module. This was not used for creating the basic design, but the potential of the additional functionality is elaborated upon in section 3.2.

2.3 Natural frequency check

The 10 MW turbine has an operational range of 6-9.6 rpm. Hence, the 1P frequency band is from 0.10-0.16 Hz and the 3P frequency band 0.30 – 0.48 Hz. The fundamental frequency of the entire support structure should be minimum 10% above 1P max (i.e. pass if $f_1 > 0.176\ Hz$).

In this section, an analytical expression is searched for that can deliver an accurate instantaneous value of the first natural frequency such that the designer can adjust the diameter on the fly.

As a first approximation of the first natural frequency a lumped mass on a stick model can be used as presented in the PhD thesis of van der Tempel [3]. However, this does not take into account the variation of flexural rigidity and mass over the height. And since the diameter of the proposed design tapers from 9.6 to 4.2 m the point-on-a-stick model is considered not accurate enough.

Alternatively, the analytical expression for a Rayleigh stepped tower may be used to approximate the natural frequency. This method determines the unit mass and inertia per discrete section and introduces an expected mode shape. In Appendix A the expressions and principles for this method are worked out further.

Figure 4: 'Point on a stick' model [3]

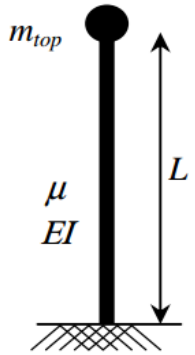

Figure 5: Rayleigh stepped tower [4]

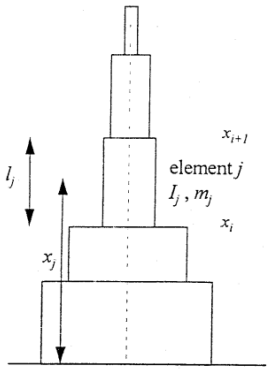

The Rayleigh stepped tower method results in a first natural frequency of 0.245 Hz, including the added mass of the submerged sections and foundation stiffness (see **Table 3**).

In Phatas, the natural frequency of the support structure is a result of the Craig-Brampton modelling and is reported in towmod output files. As detailed loadcase calculations will be performed with Phatas, the towmod natural frequency is compared to the Rayleigh stepped tower in **Table 4**.

The frequency of 0.199 Hz is larger than 0.176 Hz and thereby passes the natural frequency check. It must be noted that the Rayleigh stepped tower model shows a distinctively higher eigenfrequency. This is cause of concern and deserves further attention. For now, the natural frequency for both methods passes the natural frequency check.

Table 4: Natural frequency estimation

	Phatas towmod	Rayleigh stepped tower
Rev00	0.199 Hz	0.245 Hz

2.4 Extreme load check (yield and buckling)

The local loads are expressed in three components: N for the axial (compressive) force, V for the shear force (positive downwind), and M for the (effective) fore-aft bending moment. For the design of the monopile, ultimate loads are evaluated by taking into account the maximum rotor thrust force, self-weight of the support structure and rotor-nacelle assembly, and hydrodynamic loading of the 50 year extreme wave. This combination is conservative as it combines the maximum turbine load (when in operation) with the maximum hydrodynamic load from a 50 year extreme wave. In case

this sea state occurs, probably the turbine is idling. The combination is therefore not prescribed by the IEC standard [5].
Only the extreme thrust force and self-weight of the rotor nacelle assembly are applied at the tower top.

Thrust force
The maximum thrust force as reported in [6] is 4605 kN including a load safety factor γ_F of 1.35. A comparison is shown in **Table 5**. The DTU thrust force is considered to be unrealistic because the ultimate loads have been extrapolated to a 50 year ultimate value. Instead, the DTU 10 MW RWT has been modelled by ECN in aero-elastic load simulation tool Phatas in the Focus6 suite. A set of 828 loadcases has been calculated for an onshore and offshore model in 35 m water depth as created in other projects, for which the maximum (absolute) thrust force is shown in **Table 5**. The value of the 35 m monopile will be used further in the report and is hence indicated in bold writing in **Table 5**.

Table 5: Maximum (absolute) thrust force

	$\max\lvert F_{thrust}\rvert\ [kN]$	Includes γ_F?
DTU onshore, at V=11 m/s	1508	No
DTU onshore, max (DLC 1.3)	4605	Yes
ECN trendwatcher, onshore (DLC 1.3, 12 m/s)	2442	No
ECN trendwatcher, offshore, monopile 35 water depth (DLC 1.3, 12 m/s)	**2419**	No

Applying the thrust force results in an internal shear force V that is constant over the height of the support structure and an increasing bending moment M to the mudline.

Self-weight
The rotor-nacelle assembly of the 10 MW RWT has a mass of 674 tons [6]. The self-weight of the support structure and the weight rotor-nacelle assembly are multiplied by a constant load factor of 1.25 to determine the local axial force N as prescribed by DNV for a static load .

Hydrodynamic loading
The hydrodynamic loading has been estimated by means of a simple calculation as applied in the Upwind cost model [7]. The 50 year extreme wave height for the given site is 17.67 m. The corresponding significant wave height is determined by Equation 1. The period is found by Equation 2.

$$H_{red} = 1.1 * H_{50yr}/1.86 \qquad \text{Equation 1}$$

$$T_{red} = 11.1\sqrt{\frac{H_{red}}{g}} \qquad \text{Equation 2}$$

The Morison equation is used for a first estimate of the extreme loads[1]. It contains a drag term and an inertia term. Below, drag coefficient $C_D = 1$, inertia coefficient $C_M = 2$ and water density $\rho_w = 1025\ kg/m^3$.

$$F_{hyd}(z_i, t) = F_d(z_i, t) + F_i(z_i, t) \quad \text{Equation 3}$$

$$F_D(z_i, t) = \left(z_{i,top} - z_{i,bottom}\right) \cdot \frac{1}{2} \rho_w \cdot C_D \cdot D_i \cdot u_n(z_i, t) \cdot |u_n(z_i, t)| \quad \text{Equation 4}$$

$$F_i(z_i, t) = \left(z_{i,top} - z_{i,bottom}\right) \cdot \frac{\pi}{4} \rho_w \cdot C_M \cdot D_i^2 \cdot \dot{u}_n(z_i, t) \quad \text{Equation 5}$$

Velocity $u_n(z_i, t)$ and acceleration $\dot{u}_n(z_i, t)$ follow the airy wave theory, where the motion of the water particles at section i for wave n can be described by the following set of equations.

$$u_n(z_i, t) = \zeta_n \cdot \omega_n \cdot \frac{\cosh(k_n\, z_i)}{\sinh(k_n d)} \cdot \sin(\omega_n t) + u_c(z_i) \quad \text{Equation 6}$$

$$\dot{u}_n(z_i, t) = \zeta_n \cdot \omega_n^2 \cdot \frac{\cosh(k_n\, z_i)}{\sinh(k_n d)} \cdot \cos(\omega_n t) \quad \text{Equation 7}$$

Where ζ_n is equal to $H_{red}/2$, ω_n is the wave frequency in rad/s, d is the water depth, $u_c(z)$ is the current velocity, and k_n is the angular wave number which is iteratively determined by Equation 8.

$$k_n = \frac{\omega_n^2}{g \tanh k_n d} \quad \text{Equation 8}$$

$u_n(z_i, t)$, $\dot{u}_n(z_i, t)$, $F_d(z_i, t)$ and $F_i(z_i, t)$ are determined for each section for which the average height z_i is lower than LAT. The hydrodynamic force $F_{hyd}(z_i, t)$ is found for a water depth of 29.6 m with a uniform current profile u_c of 1.2 m/s and 50 yr extreme wave conditions ($H_{red} = 10.45\ m$, $T_{red} = 11.46$ s). The maximum $F_{hyd}(z_i)$ in one wave period is added to internal shear force V after multiplication with variable load factor γ_F of 1.35. The wave loading also influences the distribution of the internal bending moment M.

1 Note that for the fatigue simulations, kinetics and hydrodynamic loads of the waves, including current, are calculated by random ocean wave simulation tool ROWS [5]

Figure 6: Internal loads distribution for extreme thrust force and 50 year extreme wave

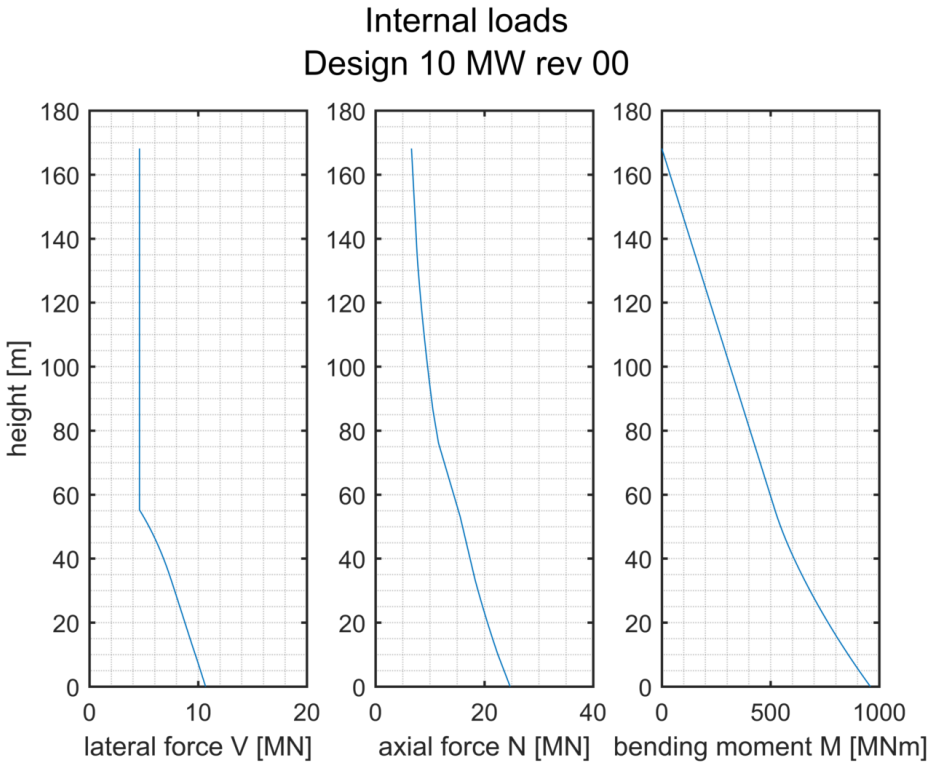

2.4.1 Yield check

The yield check considers whether the local stress is smaller than the yield strength S_y. If the condition in Equation 9 the yield check is passed.

$$\frac{N}{A} + \frac{M}{W_e} \leq \frac{S_y}{\gamma_M} \qquad \text{Equation 9}$$

Where W_e is the (elastic) section modulus that can be evaluated by Equation 10.

$$W_e = \frac{I}{y} = \frac{I}{D/2} = \frac{\pi}{32}\left(\frac{D^4 - (D-2t)^4}{D}\right) = \frac{\pi}{32}D^3\left[1 - \left(1 - \frac{2t}{D}\right)^4\right] \qquad \text{Equation 10}$$

Yield strength S_y is set at 355 MPa for monopile, transition piece and tower (as reported in [6]). A material safety factor $\gamma_m = 1.1$ is used in Equation 9.

As can be seen in **Figure 7**, the stress throughout the structure is lower than the yield stress divided by the material safety factor. Hence, no yield failure is expected and the yield check is passed.

Figure 7: Local stress (blue line)

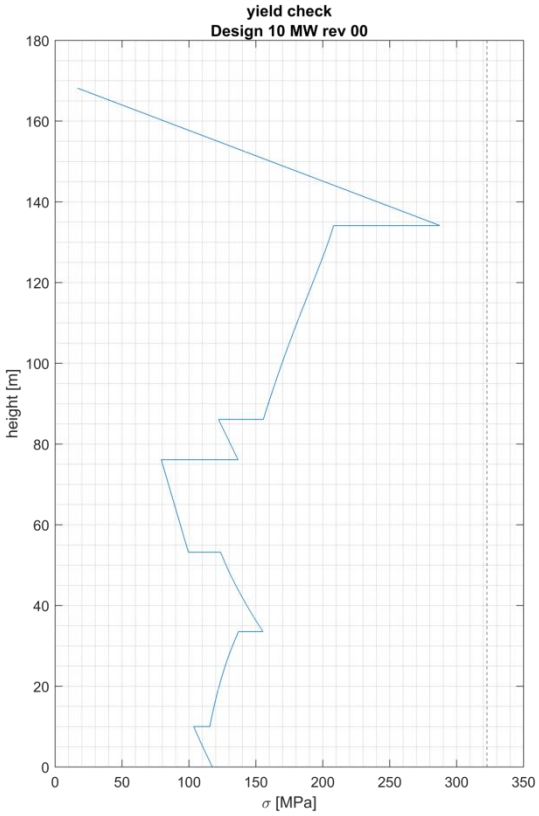

2.4.2 Global buckling check

The global buckling check is performed to determine column buckling of the entire support structure (monopile, transition piece and tower). The equations used for this check are presented in Appendix B. The parameter β determines the buckling mode, displayed in **Figure 8**. It is anticipated that $\beta = 2$ is the failure mode for the entire support structure. However, as can be seen by the right plot in **Figure 9**, the global buckling check is not passed for $\beta = 2$ (global buckling utilization ratio is above 1, equaling a buckling failure).

Figure 8: Buckling failure modes

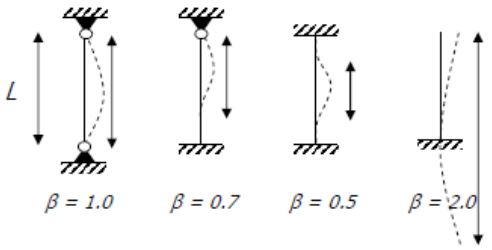

Figure 9: Global buckling check for two buckling failure modes

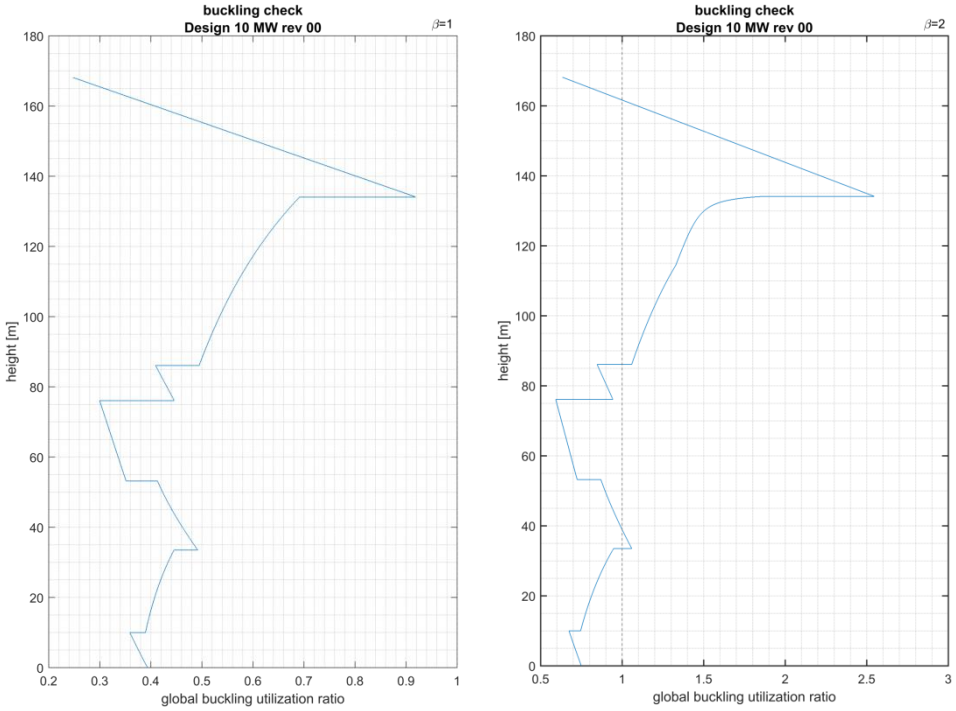

The validity of this buckling mode for the entire support structure is subject to further evaluation considering that there are several flanges (and a stiff transition piece) present in the structure, which can resist a global buckling mode as shown in **Figure 8**.

2.4.3 Local buckling check

In 'Theory of elastic stability' of Timoshenko & Gere [8], the critical local buckling stress is given with Equation 11.

$$\sigma_{cr} = \frac{E\ t_w}{0.5D\sqrt{3(1-\nu^2)}} = \frac{N_{crit}}{A} \qquad \text{Equation 11}$$

According to DNV OS C201 [9], local buckling of tubular members with external pressure need not to be considered for

$$\frac{D}{t} \leq 0.5\sqrt{\frac{E}{S_y}}$$

Or in other words, local buckling must be checked for $\frac{D}{t} \geq 12$.

As for all sections the D/t ratio it well above 12, local buckling must be checked for each cylinder section. In **Figure 10** the critical stress and critical normal force are given. As can be seen by the yellow striped line, the critical stress and normal force are not reached by far.

Figure 10: Local buckling critical stress and normal force

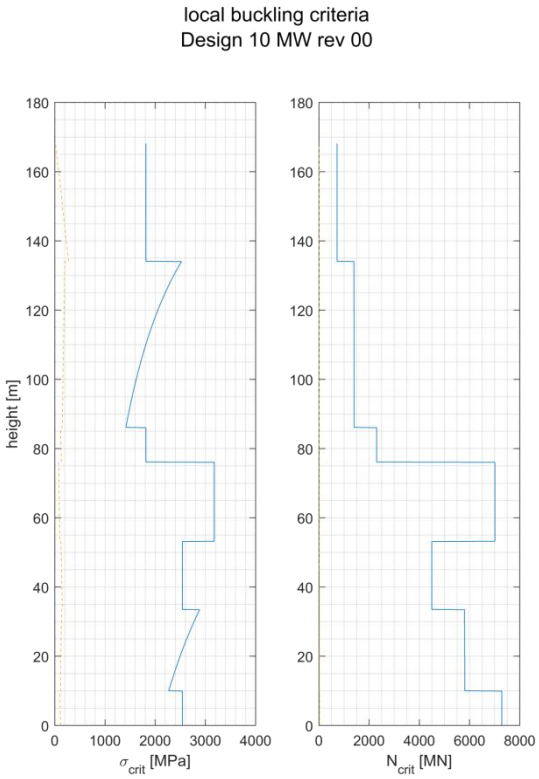

2.5 Fatigue check

2.5.1 Load case description (power production)

Design load case (DLC) 1.2 is taken for the calculation of fatigue damage, according to IEC 61400-3 [5]. This load case describes a number of seeds per wind speed bin over the operational range. Six unique seeds are used to generate the turbulent wind field for each wind speed bin, running from 3 to 25 m/s. The loadcases are prepared using the Focus program LCprep3ed1, following IEC 61400-3 edition 1 [5].

The occurrences are also calculated by LCprep and follow a Weibull distribution, defined by a Weibull shape parameter and annual average wind speed for a twenty year duration. The distribution used in fatigue processing is graphically depicted in **Figure 11**.

The environmental conditions are based on the Upwind deep water site, which is based on measurements at the K13 platform and reported upon in Upwind design basis document [10]. The reference hub height of the Upwind deep water design, annual average wind velocity at this height and roughness length is shown in **Table 6**. Because the hub height of the proposed monopile design is higher (due to the larger blade diameter), the annual average wind velocity is extrapolated using the logarithmic shear formulation in Equation 12.

$$V(z) = V(z_{ref}) \cdot \frac{\ln(z/z_0)}{\ln(z_{ref}/z_0)} \qquad \text{Equation 12}$$

Table 6: Annual average wind velocity at reference height Upwind and hub height 10 MW monopile

Upwind K13 deep water site		
z_{ref} Upwind	90.55	m (above SWL)
V (z_{ref})	10.05	m/s
z0	0.002	m
10 MW monopile		
z	121.521	M
V(z)	10.33	m/s

Figure 11: Distribution of 10 minute loadcases K13 deep [10]

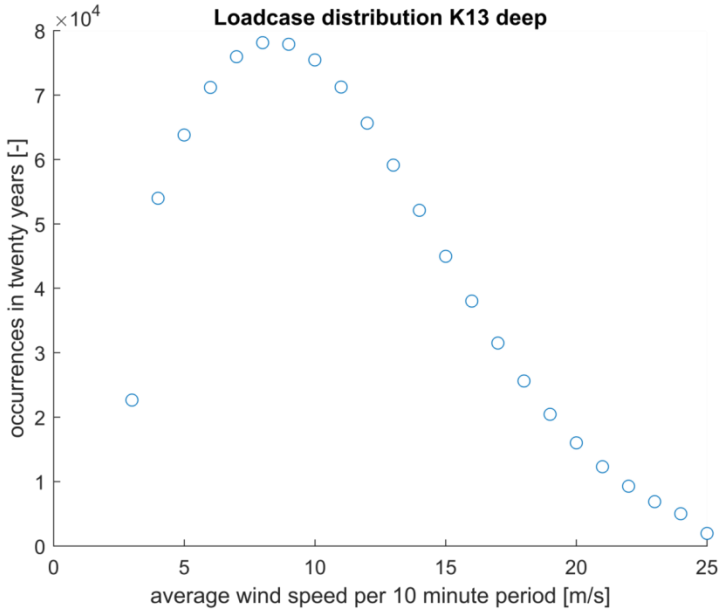

2.5.2 Fatigue processing

After simulating six ten minute time series with different wind and wave seed per (1 m/s) wind speed bin, the resulting forces and moments in the structure are post-processed into a fatigue equivalent value per loadcase. The rainflow algorithm is used to count individual cycles with distinct range ΔS_i. Since the PHATAS simulation tool does not calculate stresses, the force and bending moment time series are substituted for S. The fatigue equivalent force or moment can be found by applying Equation 13. Here N_{eq} is the equivalent number of cycles and m is the Wohler coefficient. For a ten minute time series, when choosing $N_{eq} = 600$, the resulting ΔS_{eq} is a 1Hz-equivalent fatigue range. This means that a fixed amplitude 1Hz harmonic with range ΔS_{eq} causes the same level of fatigue damage as the mixed amplitude, multi-harmonic series S(t).

$$\Delta S_{eq} = \left(\sum_{i=1}^{n} \frac{\Delta S_i^m}{N_{eq}} \right)^{1/m} \qquad \text{Equation 13}$$

2.5.3 Fatigue load DLC 1.2

As was concluded from section 2.5.2 above, fatigue equivalent loads can be post-processed by FocusReport. A set of 138 loadcases was simulated for Design Load Case 1.2, according to IEC 61400-3 [5]. Fatigue equivalent fore-aft bending moment at mudline for these loadcases is presented in **Figure 12**.

Figure 12: Fatigue equivalent bending moment (using single Wohler component m=4)

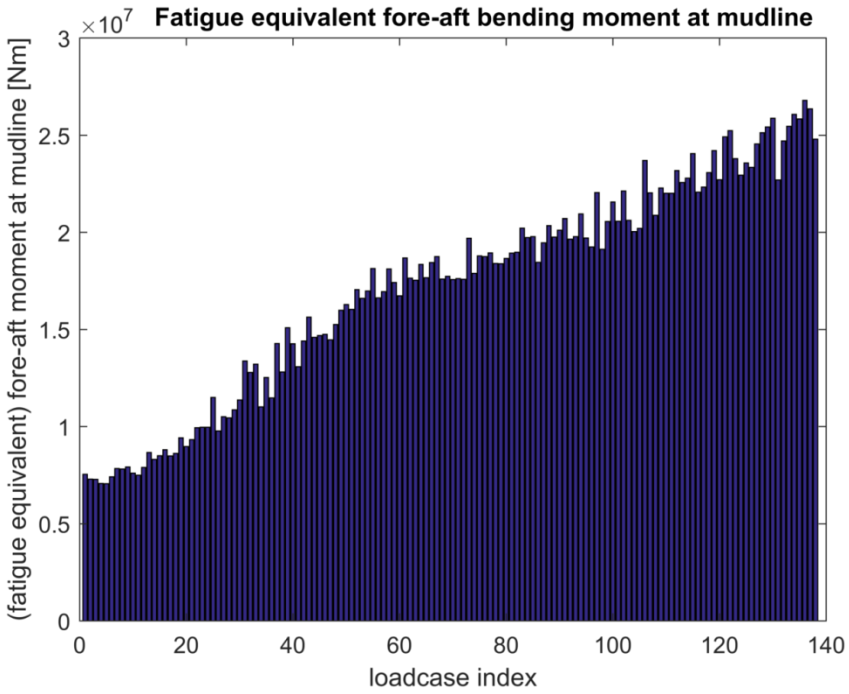

An approximation can be made to the fatigue equivalent normal stress at the mudline by evaluating the fore-aft bending moment into stress $\left(\sigma_{N\ deql} \approx \frac{M_{\mathrm{y,deql}} \cdot D_o}{2I}\right)$. However, also the normal force contributes to the magnitude of stress in the material. Equation 14 shows all contributions to normal stress. The maximum normal stress is found at the outer radius, for which the arm of the fore-aft bending moment is largest. As the fore-aft bending moment M_y is commonly larger than the sideways bending moment during power production, Equation 15 holds as an expression for maximum normal stress in a circular cross-section (for $x = D_o/2, y = 0$).

$$\boldsymbol{\sigma_N = \frac{M_x y}{I} + \frac{M_y x}{I} + \frac{N}{A}} \qquad \text{Equation 14}$$

$$\boldsymbol{\sigma_{N,max} = \frac{M_y D_o}{2I} + \frac{N}{A}} \qquad \text{Equation 15}$$

The individual contribution of fore-aft bending moment and normal force to the normal stress at the mudline is shown in a single time series of power production for 25 m/s mean wind velocity.

Figure 13: Normal stress caused by bending moment (blue) and normal force / self-weight (red) at the mudline for power production at 25 m/s mean wind velocity.

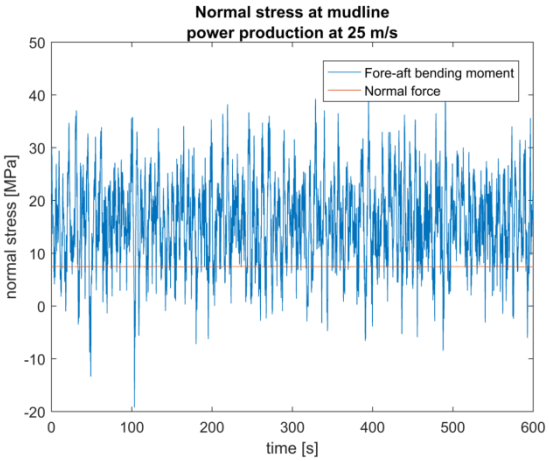

It can be seen from **Figure 13** that there is little variation in the normal stress caused by normal force, mostly consisting of self-weight of the upper structure. Hence, the contribution of normal force to fatigue is limited.

The stress time series of Equation 15 (including normal force) are rainflow counted and a damage equivalent value is created for each individual loadcase, taking into account the multi-slope SN curve, see **Figure 14**.

Figure 14: Distribution of fatigue equivalent normal stress $\sigma_{N,deql}$ at mudline, for each loadcase (upper plot) and averaged for each wind velocity (lower plot).[2]

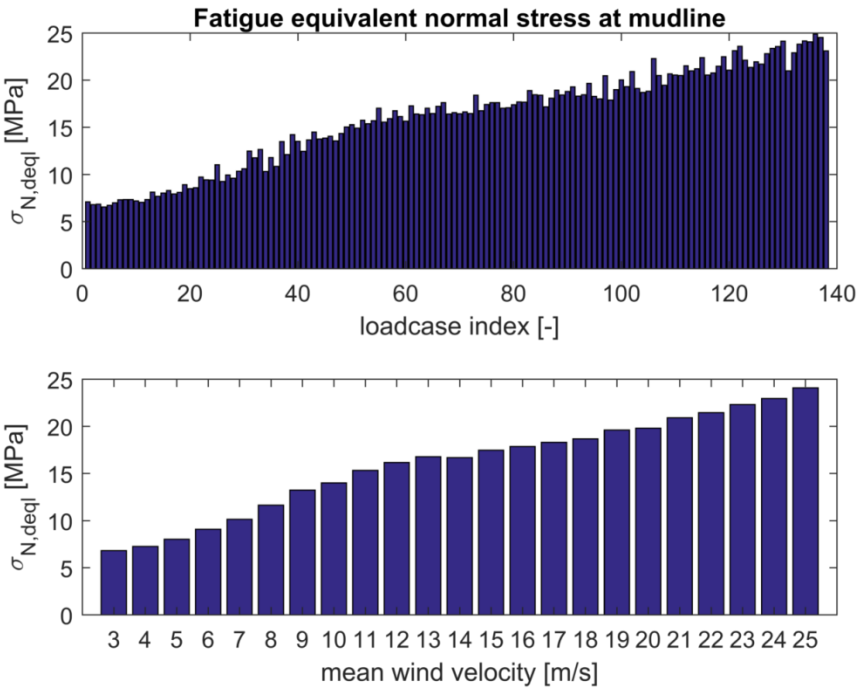

2.5.4 Fatigue damage

The fatigue damage per loadcase j is calculated by Equation 20.

$$D_j = \sum_j \frac{n_i}{N_i} \qquad \text{Equation 16}$$

For which n_i is the number of stress cycles and N_i is the number of cycles to failure for a given stress cycle range $\Delta\sigma_i$. N_i can be calculated by Equation 21, where SCF represents the stress concentration factor.

$$\log N_i = \log \overline{a} - m \cdot \log\ (\mathrm{SCF} \cdot \Delta\sigma_i) \qquad \text{Equation 17}$$

The values for $\log \overline{a}$ and m are dependent on the SN curve. According to Appendix A of DNVGL-RP_C203 Fatigue Design of Offshore Steel Structures [12], longitudinal weld seems fall under SN category B2, or C1-F3 for circumferential butt welds.

2 A multi-slope SN curve was used in creating this graph.

Table 7: S-N curves in seawater with cathodic protection (DNVGL RP C203 [12])

	$N \leq 10^6$ cycles		$N > 10^6$ cycles		
S-N curve	m_1	$\log \bar{a}_1$	m_2	$\log \bar{a}_2$	SCF
B2	4.0	14.685	5.0	93.59	N/A
C1	3.0	12.049	5.0	65.50	N/A
F3	3.0	14.576	5.0	14.576	1.61

Curve B2 is used as the representative SN relation. One has to take into account possible hot spot stresses at geometric details. An example of this is the cable entry hole, where the stress concentration factor (SCF) can be higher than 3.

The effect of plate thickness of welded joints on the fatigue damage is accounted for by multiplying the stress range by $\left(\frac{t}{t_{ref}}\right)^k$. However, for class B2, $k = 0$ and hence the thickness effect may be omitted.

For each individual loadcase, a fatigue damage D_i is calculated using Equation 16 for all identified stress ranges $\Delta\sigma_j$ in the 10 minute time series. The lifetime fatigue damage is determined by summing the individual damage times the occurrence of that loadcase, which is shown per wind speed bin in **Figure 11**. The Weibull distribution shows that the loadcases in DLC 1.2 (power production from 3-25 m/s wind speed) amount to 978780 ten minute time series, which equals 18.6 years of operation in the 20 year lifetime.

$$D = \sum \mathrm{occ}_i \cdot D_i \qquad \text{Equation 18}$$

The results for lifetime fatigue damage, for a variation of stress concentration factors, are shown in **Table 8** and **Figure 15**.

Table 8: Fatigue damage at mudline for different stress concentration factors

	SCF=1.0	SCF=1.5	SCF=2.0	SCF=2.5	SCF=3	SCF=3.5
Fatigue damage D [-]	0.0079	0.0601	0.25335	0.7721	1.9065	4.0218

Figure 15: Graph depicting fatigue damage at mudline for different stress concentration factors

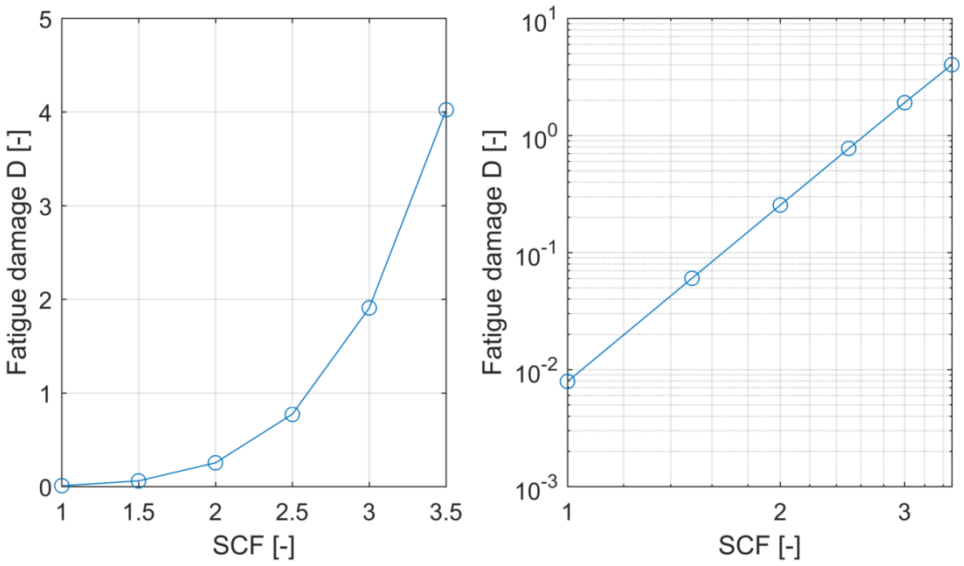

The contribution of each wind speed to the lifetime fatigue damage is found by summing the weighted damage per wind speed bin (Equation 19). **Figure 16** displays the contribution of each wind speed bin to the fatigue damage.

$$\frac{\sum_{i=1}^{6} \mathrm{occ}_i \cdot D_i}{D_{total}} * 100\% \qquad \text{Equation 19}$$

Figure 16: Contribution of each wind speed bin to total lifetime fatigue damage

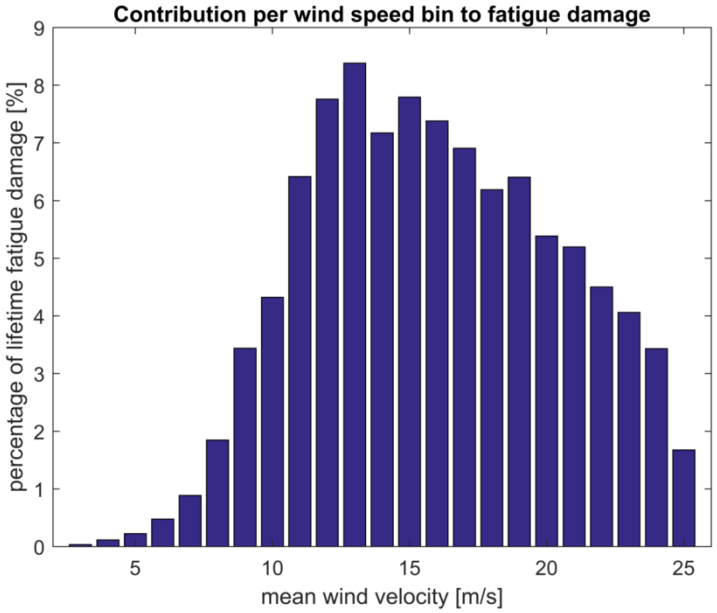

3

Limitations of current models

In this chapter, the applicability of the current modelling approach for very large monopiles is discussed. In upscaling the monopile concept, the validity of certain model assumptions may be exceeded. The modelling capabilities of the structural model, soil-structure interaction, hydrodynamic model and fatigue model are considered in this chapter.

3.1 Structural model

In Phatas a Craig-Bampton (CB) model is created to account for the tower, transition piece and monopile. This is useful in creating a beam-like model for a multi body structure such as a jacket. In order to capture the dynamics of the support structure enough CB modes must be taken into account. In the Phatas manual at least 5 internal bending modes [14] are suggested for offshore turbines and in the simulations, 6 bending modes were applied. For more information on the Craig-Bampton method, consult [15].

3.2 Soil structure interaction

Soil structure interaction is modelled in Phatas by a four degree of freedom spring matrix [14]. Recently, advances have been made to incorporate multiple springs throughout the soil making modelling of (non-linear) PY curves possible [16]. However, PY curves have been developed for slender piles in the oil & gas industry bending in an elastic fashion. A general rule of L/D ratio smaller than 7 indicates the bending mode is more rigid [17]. In the PISA project, numerical modelling and field testing was

performed and new design methods have been developed to account for large diameter foundation piles [18], [19] . The findings include the increased importance of distributed moment, base shear and base moment for shorter wider foundation piles compared to the long slender piles where lateral P-Y springs may suffice.

3.2.1 Soil stiffness models

From the investigations into the various soil-structure stiffness models, the options are listed below in increasing level of complexity:

- Rigid
- Apparent fixity length
- 2 DOF spring matrix (PHATAS)
- Linearized P-Y curves
- Non-linear P-Y curves (PHATAS + py module)
- Modified soil structure springs
- Strain wedge method
- FEM linear elastic solids
- FEM non-linear, anisotropic
- FEM multi-phase
- FEM + CFD of water

It can be seen that the additional PY module in PHATAS only increases the modelling capabilities. Because of the custom (non-linear) spring curves that can be entered, updated PY relations from the PISA project can be implemented. It is however advised to carry out a validation study, and include other degrees of freedom (vertical and rotation springs).

Influence of soil model on eigenfrequency
In the master thesis of Joey Velarde, the effect of the soil model to the natural frequency has been investigated. It turns out that the API method results in a 4.0% higher eigenfrequency than a finite element code for a 10 MW monopile foundation in 50 m water depth [20].

API method is overestimating soil stiffness, especially at greater soil depth, causing a smaller lateral deflection at the seabed and pile toe [20]. The bending moment distribution is however similar, see **Figure 17**.

Figure 17: Lateral deflection and bending moment distribution for pile of 50 m water depth [20]

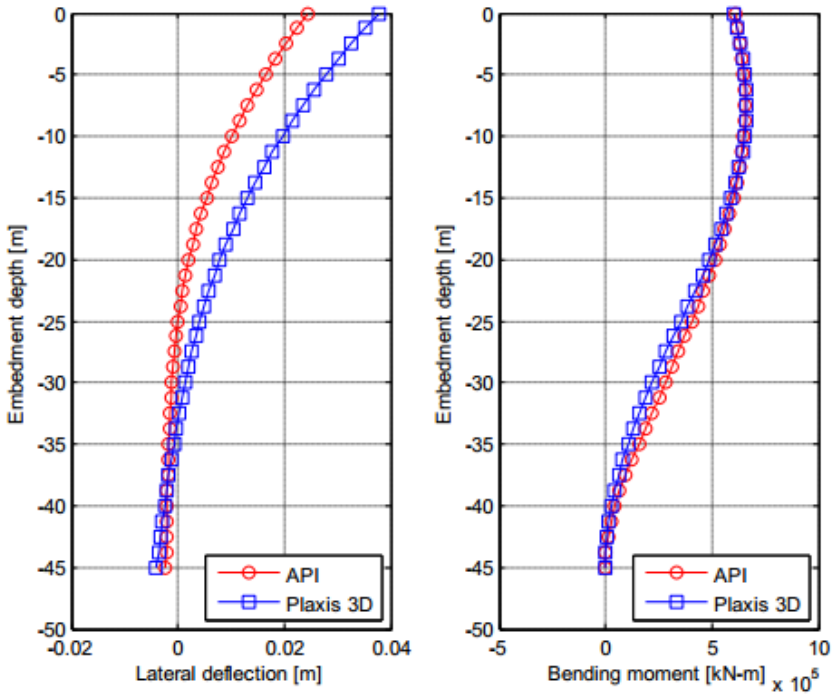

Influence of variation of soil parameters on eigenfrequency and fatigue lifetime
Sebastien Schafhirt of NTNU has carried out a soil parameter variation study for the generic NREL 5 MW turbine supported by a monopile structure as analysed in Phase II of the OC3 Project [21]. The effect on eigenfrequency, fatigue load and fatigue lifetime was quantified for a variation of soil parameters k (initial modulus of subgrade reaction), ϕ'(internal friction angle), and θ (accumulated rotation).
The fatigue lifetime was shown to vary between 18.21 – 20.80 years. A maximum reduction of 6 % for the natural eigenfrequency was found by the author.

3.2.2 Foundation damping

The effective soil damping is a value to which much uncertainty is connected. The effective soil damping influences the energy in the vibrations of the structure and as such has an influence on the simulation of cyclic loads and the resulting fatigue life. Carswell et al [22] have mapped the estimated critical damping values from literature which ranges from 0.17 % to 3 % of critical damping. ECN has conducted a study to this phenomenon in 2014 [23]. Soil damping is not modelled in Phatas however.

3.3 Hydrodynamic models: diffraction considered McCamy Fuchs

The monopile is one of the possible support structures for large sized modern wind turbines in 30-50m water depth. For these conditions the size i.e. the diameter of the monopile increases accordingly. The question is whether a XL monopile should be considered a large structure compared to the wave and wave diffraction should be accounted for.

An offshore structure is considered large in case the ratio of wave length L and the cylinder diameter D is smaller than 5 (L/D < 5). For large structures the Morison equation is not valid anymore for wave load calculations and diffraction should be accounted for. For a vertical cylinder McCamy and Fuchs (1954) [24] derived an analytical solution for the wave diffraction. The effect of diffraction can be expressed in the inertia coefficient Cm, **Figure 18**, as applied in the Morison equation.

$$C_m = \frac{4A(ka)}{\pi(ka)^2} \qquad \text{Equation 20}$$

With

$$A(ka) = \sqrt{J_1'^2 + Y_1'^2} \qquad \text{Equation 21}$$

Where a = radius of cylinder, k = wave number and J_1' and Y_1' are derivatives of the Bessel functions of the first and second kind and order 1 respectively.

Figure 18: Inertia coefficient Cm for given water depth d, wave peak period Tp and diameter D.

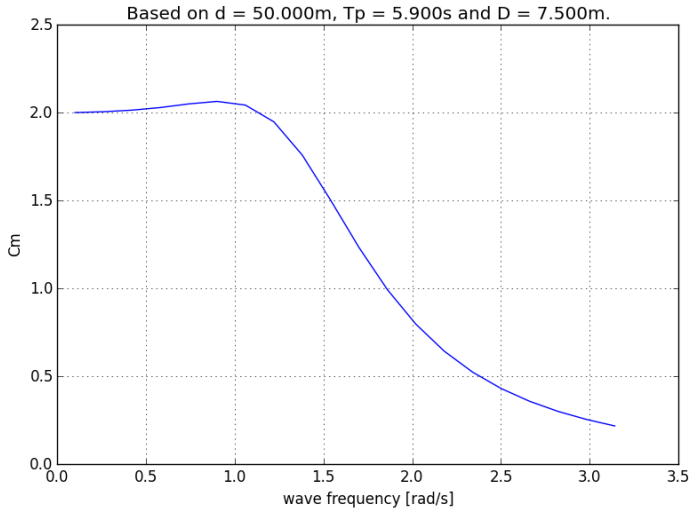

For the inertia wave load Fi and the overturning moment Mi a response amplitude operator (RAO) can be derived [25]. The equations are:

$$F_i = \rho g \frac{\pi}{4} D^2 \tanh kd \qquad \text{Equation 22}$$

$$M_i = \rho g \frac{\pi}{4} D^2 d \left[\tanh kd + \frac{1}{kd}\left(\frac{1}{\cosh kd} - 1\right)\right] \qquad \text{Equation 23}$$

Figure 19 shows the RAO of the inertia force Fi for both a constant Cm and a Cm with the McCamy Fuchs diffraction correction. For wave frequencies above 1 rad/s the effect of diffraction on the inertia force is clearly visible.

Figure 19: Inertia load Fi based on constant Cm = 2 and MacCamy Fuchs correction.

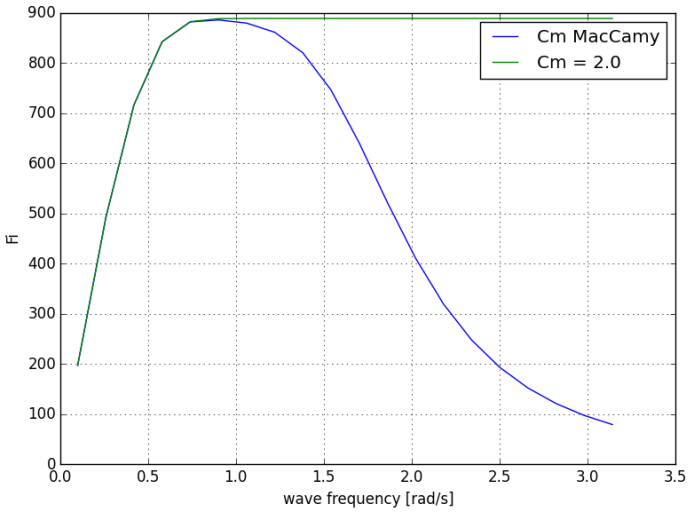

The way an offshore structure responds depends on both the wave input and the RAO of the inertia force. For a selected wave spectrum the response is calculated as follows.

$$S_{Fi} = |Fi|^2 S_\zeta \qquad \text{Equation 24}$$

Case study for three different cylinder diameters

As an example the approach is applied for three cylinder diameters: 7.5m, 10.m and 15m. The Pierson Moskowitz spectrum are applied for a seastate with significant waveheight Hs = 1.1m and a peak period Tp = 5.9s.

Based on seatate wave period Tp = 5.900s and diameter D = 7.500m. The following parameters are estimated:

- Wave number k = 0.116.
- L/D = 7.247.
- Diffracton parameter ka = 0.434.
- Inertia coefficient Cm = 2.042.

Based on the L/D number there is no need to include diffraction for this peak period. This is also confirmed by the spectral load response **Figure 20**.

Figure 20: Response spectra of inertia force Fi for a cylinder diameter D = 7.5m.

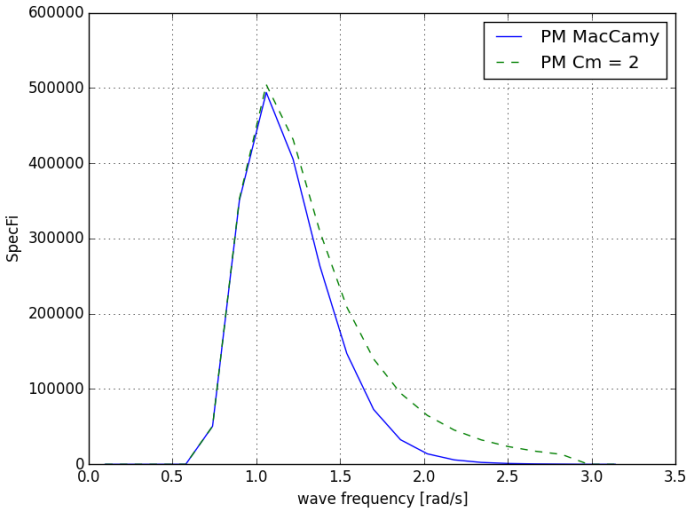

Based on sea state wave period Tp = 5.900s and diameter D = 10.000m. The following parameters are estimated:

- Wave number k = 0.116.
- L/D = 5.435.
- Diffraction parameter ka = 0.578.
- Inertia coefficient Cm = 1.940.

The L/D coefficient is now very close to five, where diffraction becomes more important. **Figure 21** shows that for the difference at higher wave frequencies becomes visible.

Figure 21: Response spectra of inertia force Fi for a cylinder diameter D = 10.0m.

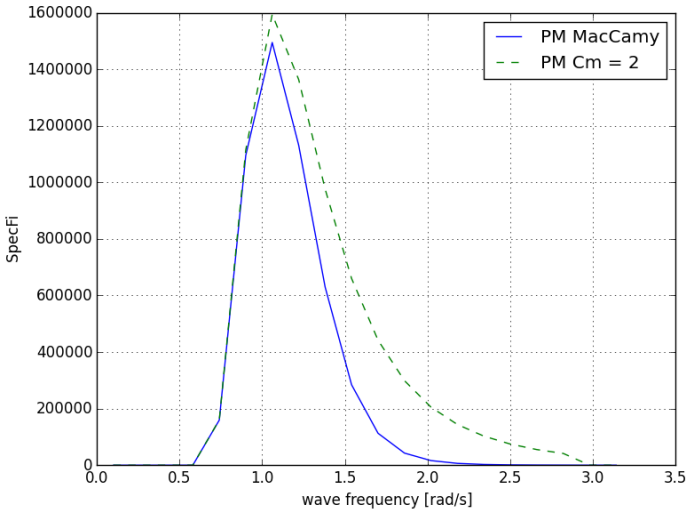

Finally based on sea state wave period Tp = 5.900s and diameter D = 15.000m.

- Wave number k = 0.116.
- L/D = 3.623.
- Diffraction parameter ka = 0.867.
- Inertia coefficient Cm = 1.561.

The L/D ratio is below five. It is clear from **Figure 22** that wave diffraction should be accounted for.

Figure 22: Response spectra of inertia force Fi for a cylinder diameter D = 15.0m.

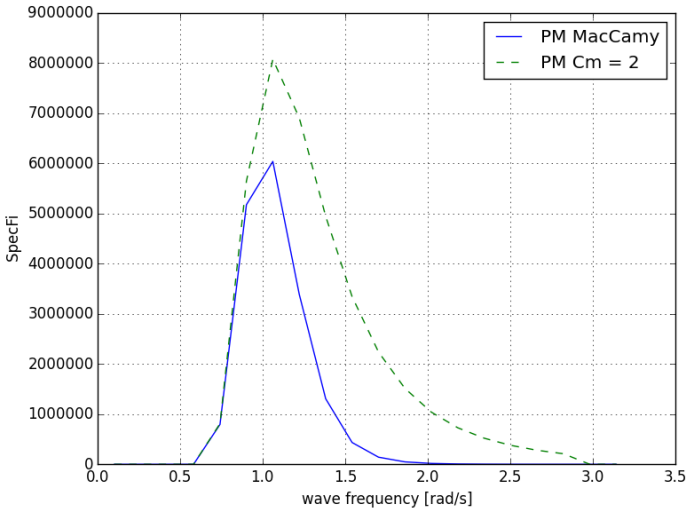

Conclusions

For a given sea state the peak period Tp can be used in the L/D ratio to identify whether diffraction should accounted for. The response spectrum shows clearly which wave frequencies are sensible to diffraction effects.

3.4 Fatigue model

In the fatigue damage evaluation of section 2.5, the SN curve has been used in conjunction with Palmgren-Miner's rule. This a commonly used approach described in DNVGL recommended practises. However, there are large uncertainties connected for this model. Both the SN parameters as the Palmgren-Miner's rule include uncertainties. In [13], the standard deviation of 0.2 for $\log \bar{a}_1$ and 0.25 for $\log \bar{a}_2$ are assumed. The Palmgren-Miner rule is assumed log normal distributed with a median 1.0 and Coefficient of Variation (CoV) of 0.3 [12]. This means that there is an inherent uncertainty on the value of fatigue damage when using this simple approach. However, the standard prescribes the use of these SN curves, which are in the end derived from experiments, together with a safety factor. Hence conservatism is introduced that could be reduced by investigating more physical effects of fatigue build-up and degradation.

For example, the assumption of linear fatigue damage over time does not account for hardening/softening effects or accelerated crack growth. More complex fatigue models have been developed to describe this effect. TNO is currently conducting a TKI Project 'FeLoSeFI' on the inclusion of retardation and load sequence effects and at institutes such as WMC and Forwind fatigue tests of joints in jackets are carried out.

4

Conclusion & Recommendations

In this report, the design procedure for a monopile support structure is presented and a basic design is created for the Innwind 10 MW offshore turbine in 50 m water depth. This combination of a large turbine in deep water has not been applied by the industry at this moment and may be considered outside the boundaries of applicability of a monopile support structure. The preliminary design suggested as a first revision is within the current manufacturing capabilities [26] with a bottom diameter of 9.3 m and a combined foundation, transition piece and tower mass of 1840 tons (excluding the embedded monopile section). Installing such an XL monopile will form a challenge. However, initial contacts with the industry have indicated that if there is a demand for larger crane capacity, hammer size or lifting reach, the installation contractors will develop new vessels that can handle such sizes.

The basic design was subjected to a quasi-static ultimate load check, buckling check and a fatigue check (at the mudline only). The static ultimate load was comprised of the maximum rotor force from a previous dataset simulation (DLC 1.3) together with a 50 year extreme sea state. This is a conservative combination. It is recommended to implement a more extensive ultimate load set that includes conditions as prescribed by the design standards (where the turbine is idling for a 50 year sea state).
The nominal stress throughout the structure does not cause yielding for the ultimate load, hence the yield check is passed. For stress concentrations however, the yield stress may be surpassed. The global buckling check for column buckling of the entire support structure is not passed for the most applicable buckling mode ($\beta = 2$). However, the total buckling length for this failure mode of twice the entire support structure length is very large and may not be relevant. For $\beta = 1$, the global buckling check is passed. Further investigation is needed to assess the applicability of this global buckling mode.

Local buckling is checked for the entire support structure and the local stress and axial force is found to be much lower than the critical stress and axial force. Fatigue damage is calculated by performing a simulation of design load case 1.2, according to IEC 61400-

3 [5], for the wind and wave climate of Doggers bank. The time series were processed by applying a rainflow algorithm, SN curve and Miner's rule. The Wohler parameters for a circumferential weld in water with cathodic protection (class B2) are taken. The fatigue check is passed up to a stress concentration factor of 2.5. Limitations in the current models include soil structure interaction, and simplifications of the structural model and hydrodynamic load calculations. The increased functionality of Phatas by using lateral springs over the length of the embedded foundation pile allow for modelling of individual P-Y springs. However, it has been shown that other physical effects should not be overlooked for large diameter foundation piles. It is hence recommended to include flexibility in more degrees of freedom and perform validation studies. The structural model and the use of Morison's equation for wave loading are considered to be sensible for large monopile foundations. Calculating lifetime fatigue by applying a Wohler curve combined with the Palmgren-Miner's rule is a conventional way of determining fatigue life and follows the current standards and norms. However, when accounting for crack growth, hardening and other effects will result in a more realistic fatigue life estimation. Finally, the Rayleigh stepped tower algorithm suggested in this report did not match the eigenfrequency from Phatas and therefore needs further investigation before integrating it in a foundation design tool.

Bibliography

[1] Offshorewind.biz, “EEW SPC rolls out world’s heaviest monopile,” Mar. 2016.

[2] P. Passon, *Derivation and Description of the Soil-Pile-Interaction Models*, IEA - Annex XXIII Subtask 2, OC3 Project, 2006.

[3] J. van der Tempel, “Design of support structures for offshore wind turbines,” TU Delft, 2006.

[4] L. Harland and J. Vugts, “Analytic expression for the first natural period of a stepped tower,” Oct. 1996.

[5] *Wind Turbines - Part 3 Design Requirements for offshore wind turbines*, IEC, 2007.

[6] C. Bak, F. Zahle, R. Bitsche, T. Kim, A. Yde, L.C. Henriksen, A. Natarajan, and M. Hansen, *DTU 10-MW Reference Wind Turbine*, 2013.

[7] W.E. de Vries, *UpWind - Final report WP 4.2 - Support Structure concepts for Deep Water Sites*, Delft University of Technology, 2011.

[8] S.P. Timoshenko and J.M. Gere, *Theory of elastic stability*, 1961.

[9] *Buckling strength of plated structures*, DNV Recommended Practise C201, 2010.

[10] T. Fischer, W. deVries, and B. Schmidt, *Upwind Design Basis - WP4: Offshore foundations and support structures*, 2010.

[11] H.B. Hendriks and B.H. Bulder, *Fatigue equivalent load cycle method - a general method to compare the fatigue loading of different load spectrums*, ECN-C–95-074, 1995.

[12] *RP-C203: Fatigue design of offshore steel structures*, DNVGL Recommended Practise C203, .

[13] S. Márquez-Domínguez and J.D. Sorensen, “Fatigue reliability and calibration of fatigue design factors for offshore wind turbines,” *Energies*, vol. 5, 2012, pp. 1816–1834.

[14] C. Lindenburg, “PHATAS Release ‘Jan-2014a’ User’s manual.”

[15] J.T. Young, *Primer on the craig-bampton method*, 2000.

[16] R. Brood, *Soil modelling in phatas with P-Y reference guide*, WMC, 2016.

[17] W.G. Versteijlen, J.M. de Oliveira Barbosa, van K.N. Dalen, and A.V. Metrikine, “Method for extracting an equivalent winkler model of the 3D dynamic soil-structure interaction or large-diameter offshore monopile foundations,” *Proceedings of XLIII International Summer School Conference APM*, 2015.

[18] B. Byrne, R. McAdam, H. Burd, G. Houlsby, C. Martin, L. Zdravkovi, D. Taborda, D. Potts, R. Jardine, and M. Sideri, “New design methods for large diameter piles under lateral loading for offshore wind applications,” *3rd International Symposium on Frontiers in Offshore Geotechnics (ISFOG 2015), Oslo, Norway, June*, 2015, pp. 10–12.

[19] B. Byrne, R. McAdam, H. Burd, G. Houlsby, C. Martin, K. Gavin, P. Doherty, D. Igoe, L. Zdravkovi, D. Taborda, and others, “Field testest of large diameter piles

under lateral loading for offshore wind applications," *Proceedings of the 16th European Conference on Soil Mechanics and Geotechnical Engineering, Edinburgh, UK*, 2015.
[20] J. Velarde, "Design of monopile foundations to support the DTU 10 MW offshore wind turbine," DTU / NTNU / TU Delft, 2016.
[21] S. Schafhirt, A. Page, G.R. Eiksund, and M. Muskulus, "Influence of soil parameters on the fatigue lifelife of offshore wind turbines with monopile support structure," *13th Deep Sea Offshore Wind R&D Conference, EERA DeepWind'2016*, 2016.
[22] W. Carswell, J. Johansson, F. Lovholt, S.R. Arwade, C. Madshus, D.J. DeGroot, and A.T. Myers, "Foundation damping and the dynamics of offshore wind turbine monopiles," *Renewable Energy*, vol. 80, 2015, pp. 724–736.
[23] K.W. Hermans, *Evaluation of modal parameters and damping from the structural response of an offshore wind substructure. ECN-WIND-2014-242*, 2014.
[24] R.C. MacCamy and R.A. Fuchs, *Wave forces on piles: a diffraction theory*, Beach erosion board corps of engineers, 1954.
[25] T. Sarpkaya and I. Isaacson, *Mechanics of wave forces on offshore structures*, van nostrand reinhold company inc., 1981.
[26] SIF group, "Monopile manufacturing State-of-the-art, https://sif-group.com/en/quality/state-of-the-art," 2016.

Appendices

Appendix A. Rayleigh stepped tower

The natural frequency of a tower with varying diameter can be approximated by the analytic expression following the Rayleigh method. This has been worked out in a note by Léon Harland and Jan Vugts in the OPTI-OWECS project [4] and was applied later in the Upwind cost model.

The method is based upon the principle of maximum potential and kinetic energy in the vibration modes and assumes a mode shape $\Psi(x)$ beforehand.
The mode shape used in the approximation can be described by Equation 25 and **Figure 23**.

$$\Psi(x) = \left(1 - \cos\left(\frac{\pi x}{2L}\right)\right) \qquad \text{Equation 25}$$

Figure 23: Assumed mode shape Rayleigh stepped tower

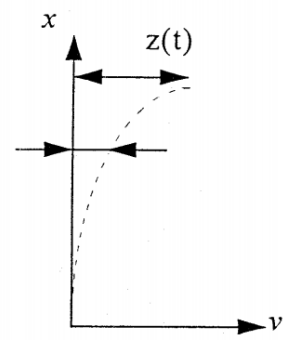

The final expression for the first natural period in the note by Harland and Vugts [4] is given in Equation 26.

$$T_t^2 = \frac{4\pi^2\left(M_{top} + m_{eq}L\right)L^3}{3EI_{eq}} \cdot \left[\frac{48}{\pi^4} + C_{found}\right] \qquad \text{Equation 26}$$

The equivalent moment of inertia I_{eq}, mass per unit length m_{eq} and foundation flexibility C_{found} is found by the next expressions:

$$I_{eq} = \frac{\sum_{j=1}^{n} I_j l_j \cos^2\left(\frac{\pi x_j}{2L}\right)}{L} \qquad \text{Equation 27}$$

$$m_{eq} = \frac{\sum_{j=1}^{n} m_j l_j \left(1 - \cos\left(\frac{\pi x_j}{2L}\right)\right)^2}{L} \qquad \text{Equation 28}$$

$$C_{found} = \frac{3EI_{eq}}{K_{eq}L} \qquad \text{Equation 29}$$

$$K_{eq} = \frac{K_{rot}K_{lat}L^2}{K_{rot} + K_{lat}L^2} \qquad \text{Equation 30}$$

Additionally, when the individual section j is submerged the mass of the internal water is added to the mass m_j. For revision 00 of the support structure design, the mass and the calculated Rayleigh stepped tower frequency is shown in **Table 9**.

Table 9: Parameters for determining Rayleigh stepped tower frequency - design rev00

	value
Mass of tower steel	1849.01 tons
Mass of internal water	2773.97 tons
Mass of tower (water + steel)	4622.97 tons
First (Rayleigh) frequency	0.2454 Hz

Appendix B. Global buckling check

The following parameters are evaluated in the Upwind cost model [2] to perform a global buckling check.

Elastic buckling force N_e

$$N_e = \frac{\pi^2 EI}{1.1\, s_k^2} \qquad \text{Equation 31}$$

Buckling length $s_k = \beta * L$.

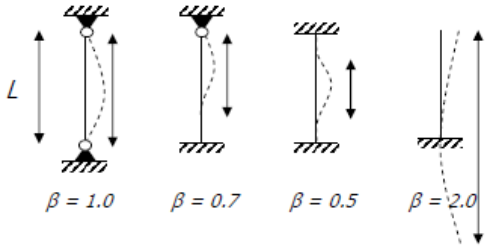

For this check, $\beta = 2.0$ and $L =$ hub height + water depth + scour depth.
The scour depth for this design is disregarded. In other words, scour protection is assumed, preventing any scour developments.

Plastic compression resistance

$$N_p = \frac{A \cdot S_y}{\gamma_M} \qquad \text{Equation 32}$$

(A: cross sectional surface area. S_y: yield strength, γ_M: material safety factor)

Plastic moment resistance

$$M_p = \frac{W_p \cdot S_y}{\gamma_M} \qquad \text{Equation 33}$$

W_p is the plastic resistance capacity or plastic section modulus and is calculated with Equation 34.

$$W_p = \frac{1}{6} D^3 \left[1 - \left(1 - \frac{2t}{D}\right)^3\right] \qquad \text{Equation 34}$$

Reduced slenderness ratio $\bar{\lambda}$

$$\bar{\lambda} = \sqrt{\frac{N_p \cdot \gamma_M}{N_e}} \qquad \text{Equation 35}$$

Determine ϕ

$$\phi = 0.5 \cdot \left[1 + \alpha \cdot \left(\bar{\lambda} - 0.2\right) + \bar{\lambda}^2\right] \qquad \text{Equation 36}$$

(α: 0.21 for hollow circular sections)

Reduction factor κ

$$\kappa = \begin{cases} \dfrac{1}{\phi + \sqrt{\phi^2 - \bar{\lambda}^2}} & \text{for } \bar{\lambda} > 0.2 \\ 1 & \text{for } \bar{\lambda} \leq 0.2 \end{cases} \qquad \text{Equation 37}$$

$$\Delta n = 0.25 \cdot \kappa \cdot \bar{\lambda}^2 \leq 0.1 \qquad \text{Equation 38}$$

Unity check buckling due to axial loading

$$\frac{N}{\kappa \cdot N_p} + \frac{\beta_M \cdot M}{M_p} + \Delta n \leq 1 \qquad \text{Equation 39}$$

Note that Equation 39 has similar features to the yield check in in Equation 9. Due to the introduction of factors κ, β_M and Δn in the equation, the buckling criterion is stricter than the yield check. In other words; if the buckling check is passed, the yield stress will not be surpassed, so in this case the yield check can be omitted. However, a yield check remains valuable for stress concentrations around geometric details such as the cable entry hole or transition piece flange weld.

veg 3
en
nds

P.O. Box 1
1755 LG Petten
The Netherlands

4949
8338